EXPERIMENTAL STUDY ON EARTHQUAKE RESPONSE OF MODELS OF PRECAST R.C. FLAT SLAB BUILDING STRUCTURES

Shen Ju-min (I) Li De-sen (II) Fu Ping-zun (III)

SUMMARY

The dynamic experiments of models were carried out on shaking table. Two models with shear wall and one without shear wall were made. The dimensions of models with five stories, two spans and two bays, are in one tenth scale of the real structure. The analysis of earthquake response was performed. It is indicated that the experimental and analytical results in the elastic and inelastic stages are in good agreement. In this paper the seismic behavior of such structures is also discussed.

INTRODUCTION

In recent years, precast reinforced concrete frames of the flat-plate type (slab-column system) have been used extensively for apartment buildings in China. The use of such building structures, generally with stories about five or six, are also being used in seismic zones. The shear walls are usually used in these building structures to resist seismic loads and to provide adequate drift control. However, almost all of the flat-plate frame structures for apartment buildings constructed in China are prefabricated slabs and columns with shear walls either prefabricated or cast in situ. The elements of precast slabs, columns or shear walls are all connected in situ at the joint regions.

In order to study the earthquake performance of the precast reinforced concrete frames of the flat-plate type, the dynamic experiments of such models were carried out on shaking table, and the theoretical analysis of earthquake response was performed.

OUTLINE OF EXPERIMENTAL PROGRAM

Three models with shear walls in both longitudinal and transversal directions, in transversal direction only and without shear wall were made. Designations of the three test models are used as FDW, FFW and FNW respectively. The dimension of the models, with five stories, two spans and two bays, are in one tenth scale of the real structure. The overall configuration of the model is shown in Fig. 1. The elements of slabs, columns and shear walls all precast were connected in situ at the joint regions. The section of columns was 3.5 x 3.5 cm^2. The depth of slabs and shear walls were 1.8 and 1.0 cm respectively. The flexural steel was welded at the joint regions for continuity. The flexural

---

(I) Associate Prof. of Civil and Environmental Engineering, Qinghua University, Beijing, China

(II) Graduate Student, Qinghua University, Beijing, China

(III) Engineer of Civil and Environmental Engineering, Qinghua University, Beijing, China

reinforcement for all elements was ∅ 1.6 and ∅ 1.2 wire with a yield stress 2750-3640 kg/cm^2. Microconcrete properties of the models are summarized in Tab. 1.

The tests were carried out on a 1.1 x 0.9 m^2 electro-magnetic shaking table in the Laboratory of Engineering Structure of Qinghua University. Story weights were made of lead, and were 30 kg at the top story level and 50 kg at all other story level. Instrumentation of a test model was arranged so that absolut accelerations and displacement in plan at each story level and base were measured. Photograph of a test model appears in Fig. 2. The primary test for each model was an earthquake simulation for which a single direction of base motion was modelled after a measured earthquake acceleration record. Complementary test was measured the response to ambient and hammerblow, and the response to random base motion by white-noise process and the response to a static lateral force applied alternalety at each of five levels.

Base acceleration for earthquake simulation was modelled after the N-S component of El-Centro 1940 earthquake. Time scale of simulation was compressed by a factor of 10 so that reasonable ratio of base-motion to test structure frequencies would result. The experiments were divided into three stages: (1) the elastic stage before the cracks appeared; (2) the inelastic stage after the cracks appeared; (3) the failure stage after the yield of model.

THEORETICAL ANALYSIS

In analysis the following assumptions are used:

(1) It is assumed that stiffness in the plane of the horizontal floor is infinite. The sketch of the flat-plate framing with shear wall is shown in Fig. 3. The slab-column system is calculated as a equivalent frame.

(2) Bilinear degradation shape is used for representing the characteristics of the restoring force as shown in Fig. 4. The elastic deformation of the column under the axial force is also considered.

(3) When the bending moment M of the element reaches the yielding moment My, the plastic hinge zone will be formed and be concentrated at the ends of the element. The element can be considered as an element of variable stiffness with a rigid zone (Fig. 5).

The horizontal displacement function W is assumed to be developed as following series:

$$W(s.t) = T_i(t)\, f_i(s) \qquad \ldots\ldots (1)$$

In Eq. (1), $f_i(s)$ is the horizontal unit displacement functions, which describe the diagram of the unit displacement of the structure. $T_i(t)$ is the generalized displacement functions. In the same way, the bending moment M, shearing force Q and axial force N can also be developed as the following series:

$$\left.\begin{aligned} M(s.t) &= T_i(t)\, M_i(s) \\ Q(s.t) &= T_i(t)\, Q_i(s) \\ N(s.t) &= T_i(t)\, N_i(s) \end{aligned}\right\} \qquad \ldots\ldots (2)$$

In Eq. (2), Mi (s), Qi (s) and Ni (s) describe the diagrams of internal forces developed under the unit displacement function $f_i(s)$.

According to the principle of virtual displacements, the equation of the virtual work of the structure system under strong ground motion can be obtained as following:

$$\sum_{i}^{n}\left(m_{ji}\ddot{T}_i + c_{ji}\dot{T}_i + k_{ji}T_i \right) = q_j \qquad \ldots\ldots (3)$$

where

$$\left.\begin{aligned} m_{ji} &= \int_o^L m f_i f_j \, ds \\ c_{ji} &= \int_o^L c f_i f_j \, ds \\ k_{ji} &= \int_o^L \frac{M_i M_j}{EI} \, ds + \int_o^L \frac{Q_i Q_j}{GA} \, ds + \int_o^L \frac{N_i N_j}{EA} \, ds \\ q_j &= -\int_o^L m \ddot{W}_g f_j \, ds \end{aligned}\right\} \qquad \ldots\ldots (4)$$

and $\ddot{W}g$ - acceleration record of the ground motion.

Before determining the generalized stiffness coefficient kji of the whole structure system, the internal forces of the structure system under ith unit displacement condition should be calculated. The selection of the unit displacement functions can be arbitrary, but the relations among the unit displacement functions must be linear independent and they have to satisfy the boundary conditions. The numbers of the unit displacement functions would be determined by the degrees of freedoms of the structure system.

In analysis, the flat-plate frame with shear wall may be simplified as a multi-degree-of-freedom system with bending-shear mode. The sketch of simplified model is shown in Fig. 6.

TEST RESULTS AND COMPARISON WITH CALCULATED RESPONSES

Measured modal frequencies of the models FNW and FFW at the elastic stage before the cracks appeared and at the inelastic stage after the cracks appeared are listed in Tab. 2. It is shown that the modal frequencies decreased as cracks of the models appeared and developed. The measured frequencies obtained from the different test procedures were closed. The calculated frequencies of first and second modes are close to those obtained from tests. The fundamental frequencies measured in different test stages were normalized by divided the measured inital frequencies so that relative decreases with increasing peak acceleration of base motion would be apparent (Fig. 7). The measured damping ratios for first, second and third modes in different test stages are listed in Tab. 3. The damping ratio for first mode measured in different test stages were normalized by divided the measured initial damping ratio as shown in Fig. 8. It is indicated that the damping ratio increases when cracks spread through a test model. The distributions of displacement response to different simulation, to lateral force at top level and measured first mode shapes are plotted in Fig. 9. It is shown that the displacements response for FNW and FFW mainly depend on fundamental mode of vibration. The measured effective width coefficient of equivalent beam of flat-plate frame was 0.53 and 0.75 respectively for FNW and FFW It is shown that the arrangment of shear wall considerably affects the effective width of equivalent beam in the flat-plate frame. Fig. 10, 11 and 12 show measured and calculated maximum response quantities for FNW

during the earthquake simulations in which peak base accelerations were 0.16g, 0.79g and 1.5g respectively. The cracks were not observed in FNW during simulation with peak base acceleration 0.16g. The cracks appeared in FNW during simulation with peak base acceleration 0.79g. Measured and calculated maximum response quantities for FFW during simulation in which peak base accelerations were 0.34g and 1.0g respectively are shown in Fig. 13 and 14. During simulation with peak base acceleration 1.0g the cracks were observed in the shear wall of the model FFW. From those above figures, it is shown that the lateral displacement of the model without shear wall was larger than that of the models with shear wall in both elastic and inelastic stages. The total shear force at the base of the model structure without shear wall was decreased greatly in both elastic and inelastic response. The results obtained from elastic and inelastic response analysis by idealized and simplified models are colse to those obtained from corresponding earthquake simulation. Fig. 15(a) shows calculated position and order of appearance of plastic hinge and the curvature ductility factor in the model FNW during simulation with peak base acceleration 1.5g. Fig. 15(b) also shows observed cracks following this simulation. It is shown that observed cracks correlated well to calculated position of the plastic hinges. For FNW maximum residual crack widths of the columns were 0.5mm following last simulation with peak base acceleration 1.85g. Fig. 16 shows the collapse of the model FFW following steady-state test in which the base motion was acceleration-controlled, sinusoidal motion at constant amplitude of 0.75g. Frequency of motion was increased in steps from below to above the apparent fundamental resonance frenquency of the model. During this test the sliding was occurred at the wall base. The horizontal cracks were formed at first, second and third floor horizontal joint between shear walls. The slab-column connecting joints were damaged at lower stories.

CONCLUSIONS

(1) Due to the inherent low stiffness of prefabricated slab-column system, shear wall may be required to provide adequate drift control and to resist seismic loading.

(2) The weaker parts of prefabricated slab-column-shear wall structure were located at the horizontal joints between shear walls and slab-column connecting joints.

(3) With the development of inelastic deformation, the stiffness of the test structure decreased, the period of vibration elongated and the damping ratio increased.

(4) Based on the assumption of equivalent frame, for the flat-plate framing with or without shear wall the experimental and analytical results in both elastic and inelastic earthquake response are in good agreement.

REFERENCES

1. Fred Allen and Peter Darvall, Lateral Load Equivalent Frame, Journal of the ACI, Vol. 74, No. 7, July, 1977, pp. 294-299.

2. Carpenter, J.E., Kaar, P.H. and Corley, W.G., Design of Ductile Flat Plate Structures to Resist Earthquake, Proc. fifth world Conf. Earthquake Engng., Vol. 2, Rome, Italy.

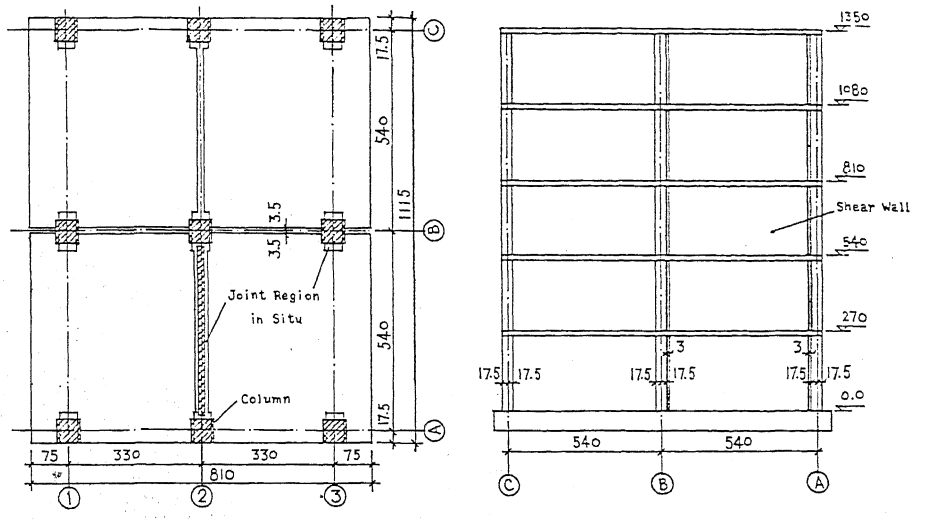

Fig. 1 Configuration of Model (Unit: mm)

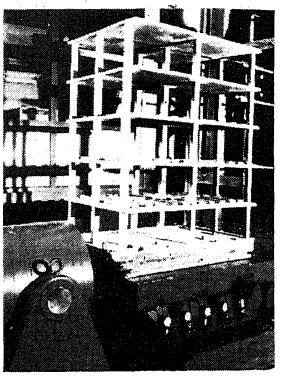

Fig. 2

Table 1 Microconcrete Properties

Model	Cement Strength (kg/cm^2)	Cement: water: Sand (weight)	Cubic Strength (kg/cm^2)	Initial Modulus (kg/cm^2)
F D W	425	1: 0.50: 2.50	471	2.72×10^5
F F W	425	1: 0.50: 2.50	471	2.72×10^5
F N W	325	1: 0.4 : 1.89	307	2.41×10^5

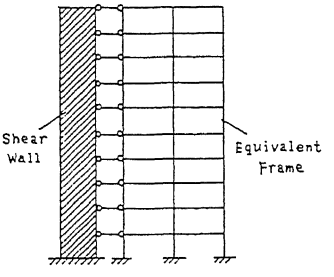

Fig. 3

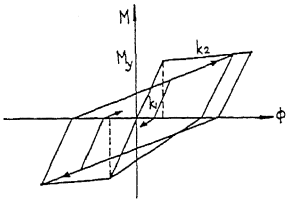

Fig. 4

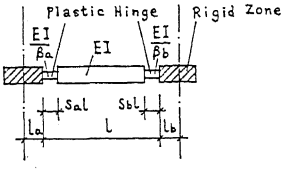

Fig. 5

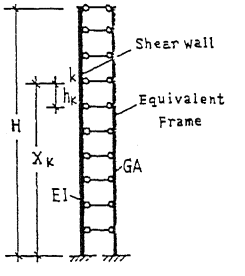

Fig. 6

Table 2 Comparison of Frequencies

Model			F N W			F F W		
Frequencies (Hz)			f_1	f_2	f_3	f_1	f_2	f_3
Uncracked	Calculated(1)		8.7	28.5	54.3	25.9	117.5	268.0
	Calculated(2)		8.8	25.6	40.7	23.5	98.7	268.2
	Measured	Ambient	9.2	29.6	--	27.3	--	--
		Excited	8.8	23.4	38.6	27.3	99.5	189.2
		Static	8.8	26.8	41.9	26.4	102.3	186.3
Cracked	Calculated(1)		7.2	22.9	41.7	18.7	99.5	267.8
	Measured		7.4	22.5	37.6	21.5	83.9	150.1

(1)-- Idealized Model; (2)-- Simplified Model.

Table 3 Measured Damping Ratio (%)

Model	F N W			F F W		
	ζ_1	ζ_2	ζ_3	ζ_1	ζ_2	ζ_3
Initial	7.2	3.6	2.5	1.7	2.1	5.1
Uncracked	7.9	4.2	2.8	1.8	3.3	5.6
Cracked	9.1	5.4	3.4	2.0	5.9	8.2

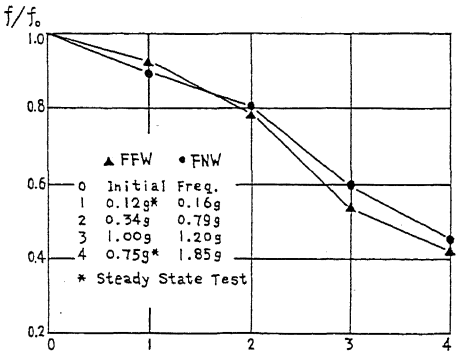

Fig. 7 Fundamental Frequency Variation

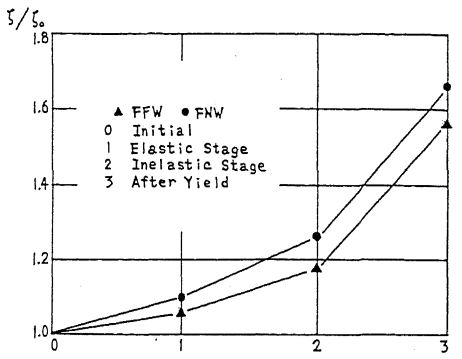

Fig. 8 Damping Ratio Variation (First Mode)

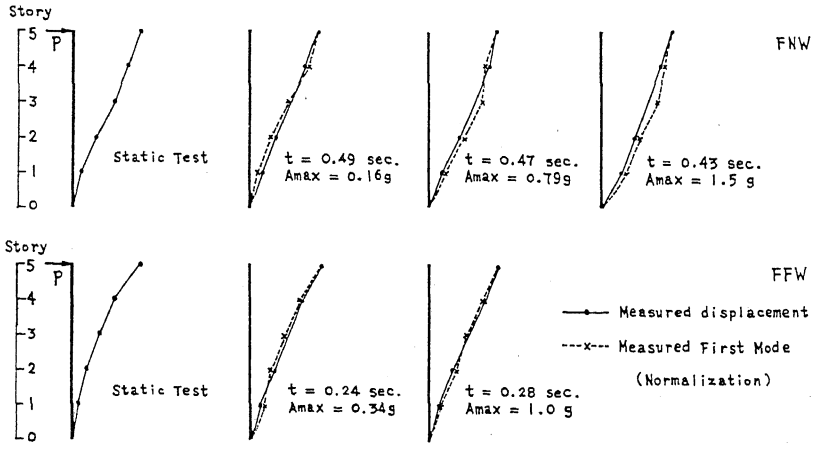

Fig.9 Measured Displacement Curve during Static Test and Simulation

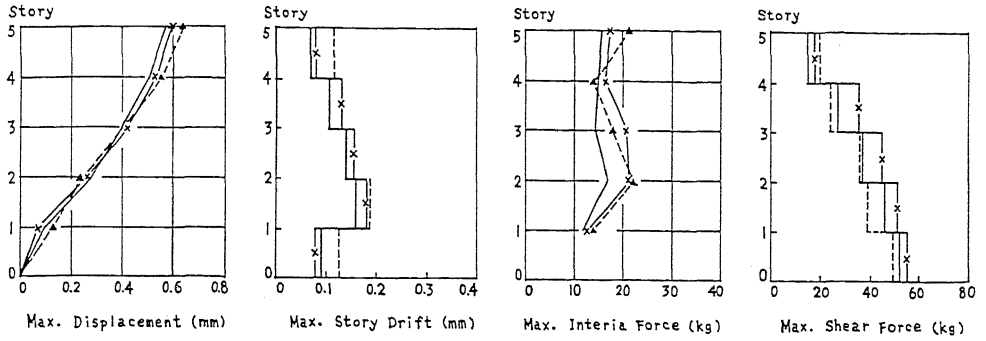

Fig.10 Maximum Response Quantities For FNW (Amax= 0.16 g)

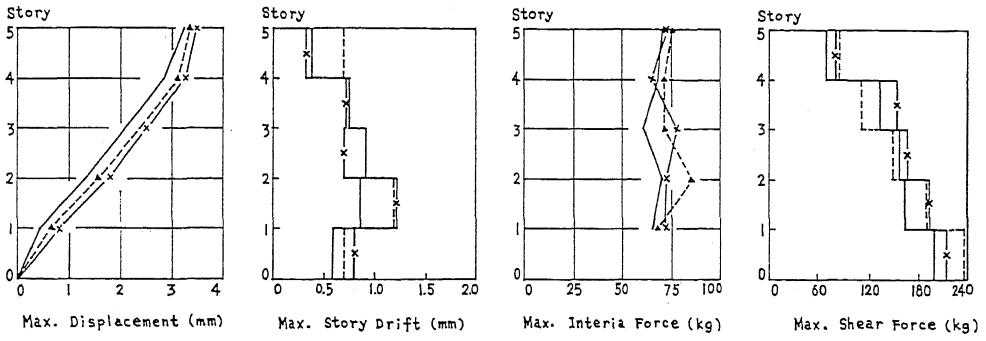

Fig.11 Maximum Response Quantities For FNW (Amax= 0.79 g)

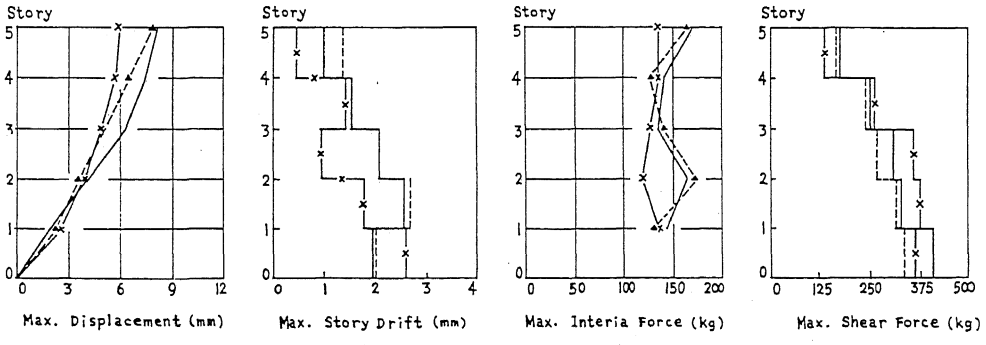

Fig.12 Maximum Response Quantities For FNW (Amax= 1.50 g)

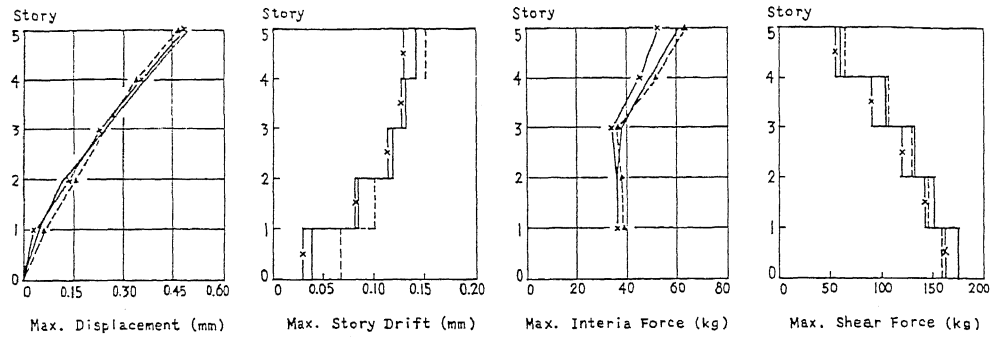

Fig.13 Maximum Response Quantities For FFW (Amax = 0.34 g)

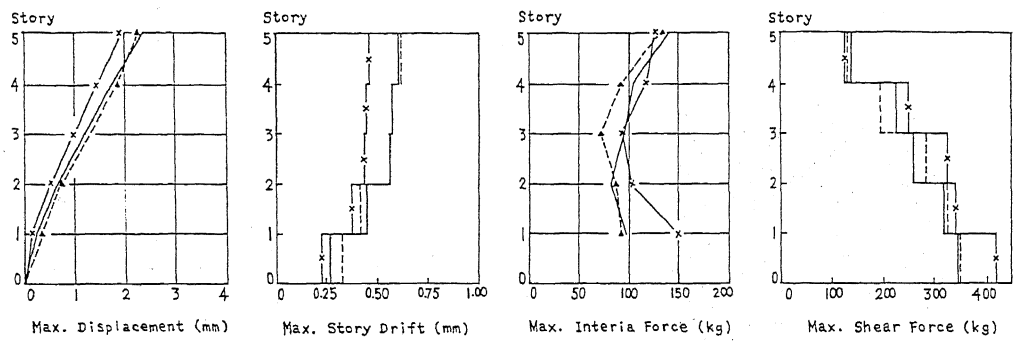

Fig.14 Maximum Response Quantities For FFW (Amax = 1.0 g)

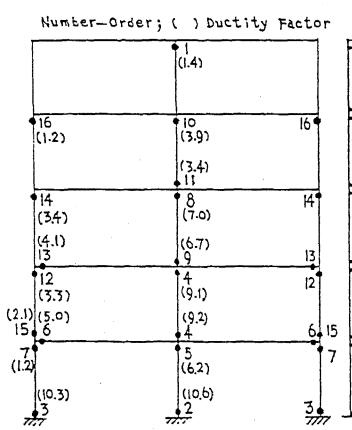

Fig.15a Calculated Yield Mechanism (FNW) (Amax = 1.5 g)

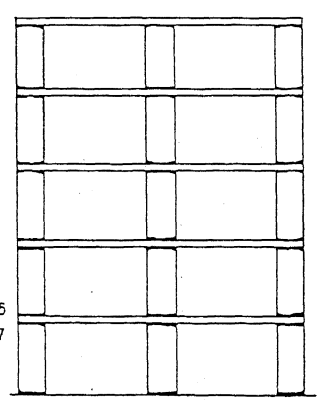

Fig.15b Cracks Observed Following Simulation Amax=1.5g (FNW)

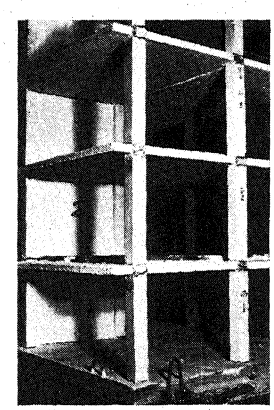

Fig.16